HHS Public Access

Author manuscript

ACS Appl Mater Interfaces. Author manuscript; available in PMC 2019 August 08.

Published in final edited form as:

ACS Appl Mater Interfaces. 2018 August 08; 10(31): 26016–26027. doi:10.1021/acsami.8b07632.

Rapid Bioorthogonal Chemistry Enables *in Situ* Modulation of Stem Cell Behavior in 3D without External Triggers

Ying Hao[#1], **Jiyeon Song**[#1], **Anitha Ravikrishnan**[1], **Kevin T. Dicker**[1], **Eric W. Fowler**[1], **Aidan B. Zerdoum**[2], **Yi Li**[3], **He Zhang**[1], **Ayyappan K. Rajasekaran**[4], **Joseph M. Fox**[1,3,*], and **Xinqiao Jia**[1,2,*]

[1.]Department of Materials Science and Engineering, University of Delaware, Newark, DE, 19716, USA

[2.]Department of Biomedical Engineering, University of Delaware, Newark, DE, 19716, USA

[3.]Department of Chemistry and Biochemistry, University of Delaware, Newark, DE, 19716, USA

[4.]Therapy Architects, LLC, Helen F Graham Cancer Center, Newark, DE, 19718, USA

[#] These authors contributed equally to this work.

Abstract

Chemical modification of engineered microenvironments surrounding living cells represents a means for directing cellular behaviors through cell-matrix interactions. Presented here is a temporally controlled method for modulating the properties of biomimetic, synthetic extracellular matrices (ECM) during live cell culture employing the rapid, bioorthogonal tetrazine ligation with *trans*-cyclooctene (TCO) dienophiles. This approach is diffusion-controlled, cytocompatible and does not rely on light, catalysts or other external triggers. Human bone-marrow-derived mesenchymal stem cells (hMSCs) were initially entrapped in a hydrogel prepared using hyaluronic acid carrying sulfhydryl groups (HA-SH) and a hydrophilic polymer bearing both acrylate and tetrazine groups (POM-AT). Inclusion of a matrix metalloprotease (MMP)-degradable peptidic crosslinker enabled hMSC-mediated remodeling of the synthetic environment. The resultant network displayed dangling tetrazine groups for subsequent conjugation with TCO derivatives. Two days later, the stiffness of the matrix was increased by adding chemically modified HA carrying multiple copies of TCO (HA-TCO) to the hMSC growth media surrounding the cell-laden gel construct. In response, cells developed small processes radially around the cell body without a significant alteration of the overall shape. By contrast, modification of the 3D matrix with a TCO-tagged cell-adhesive motif caused the resident cells to undergo significant actin polymerization, changing from a rounded shape to spindle morphology with long cellular processes. After additional 7 days of culture in the growth media, quantitative analysis showed that, at the mRNA level, RGD tagging upregulated cellular expression of MMP1, but downregulated the expression of collagen I/III and tenascin C. RGD tagging, however, was not sufficient to induce the classic osteoblastic, chondrogenic, adipogenic, or fibroblastic/

[*]Corresponding authors: jmfox@udel.edu, xjia@udel.edu.

Supporting Information: Synthesis of hydrogel precursors, homogeneity of the hydrogel network, enzymatic degradation of the primary Michael network, photographs capturing the establishment of tetrazine network, confocal and bright field images of various cell/gel constructs. This material is available free of charge via the Internet at http://pubs.acs.org.

myofibroblastic differentiation. The modular approach allows facile manipulation of synthetic ECM to modulate cell behavior, thus potentially applicable to the engineering of functional tissues or tissue models.

Keywords

Michael addition; tetrazine ligation; hydrogel; synthetic extracellular matrices; mesenchymal stem cells

1. Introduction

Synthetic hydrogels that exhibit tissue-like properties and display essential extracellular matrix (ECM) signals provide cell-instructive microenvironments to support cell growth, guide cell differentiation and promote the *in vitro* assembly of functional tissues.[1–2] Custom-designed hydrogels that are chemically diverse, mechanically tunable and biologically active have been shown to elicit diverse responses from the resident cells.[3–4] It is widely recognized that tissues and cells are dynamic entities with functions that evolve over time and are modulated through intimate cell-matrix interactions in a spatiotemporal fashion. The development of a biomimetic platform that can be modified *in situ* during live cell culture in 3D may provide fundamental insight into the changes that occur during tissue morphogenesis and in pathological cellular adaptation. Recent efforts have resulted in a number of approaches to the development of dynamic, adaptable and responsive synthetic matrices.[5–9] In some cases, matrix properties evolve passively as a result of reversible covalent crosslinks.[10] In other cases, external triggers, such as UV irradiation[11–12] or temperature/pH jumps,[7–9] have been used to induce desired changes. While light-based methods for modifying matrix properties are broadly used and effective, the cytocompatibility with light and photosensitizers is cell type dependent.[13–14] Complementary methods for modifying the synthetic ECM with temporal control would represent a valuable addition to the tissue engineering field.

We envisioned that rapid bioorthogonal chemistry could be used to modulate the extracellular microenvironment in a time-resolved and user-defined manner.[15–16] Tetrazine ligation, the cycloaddition of *s*-tetrazine (Tz) with *trans*-cyclooctene dienophiles (TCO),[17–18] is an attractive bioorthogonal reaction for such applications because it is high yielding, does not require catalysis or light and does not produce toxic side products. With a second order rate constant (k_2) that can exceed 10^6 $M^{-1}s^{-1}$ (H_2O, r.t.),[19–20] conformationally strained TCO derivatives developed in our group participate in the fastest bioorthogonal reactions recorded to date. We have successfully employed tetrazine-TCO ligation in the creation of hydrogels with well-defined spatial gradients[21] via a diffusion-controlled interfacial bioorthogonal crosslinking process without a template or external triggers. Tetrazine-TCO ligation has also been applied to the synthesis of cell-adhesive hydrogel microfibers from monomeric building blocks at the oil-water interface.[22–24] The cytocompatibility and specificity of the reaction allow matrix assembly and manipulation in the presence of cells so that the network properties can be systematically tuned to guide stem cells through stages of maturation and differentiation.

Herein, we describe a strategy to chemically modify cell-laden gel constructs in the absence of any external triggers in order to modulate the behaviors of the resident human mesenchymal stem cells (hMSCs). Our strategy (Figure 1A) utilizes a relatively slow Michael-type reaction (k_2 ~10^{-2} $M^{-1}s^{-1}$) [25] to establish a primary hydrogel network for cell encapsulation and the maintenance of 3D culture. It has been recognized that matrix mechanics can direct stem cell fate and extracellular adhesion motifs mediate cell survival and differentiation.[26–27] Through a diffusion-controlled mechanism, the network properties can be tuned by using the tetrazine-TCO ligation to increase the gel stiffness or to introduce integrin binding peptide to the primary network. As the tetrazine-TCO ligation proceeds with interfacial kinetics,[21] the modification of the 3D network is controlled only by the rate of diffusion through the cell-laden network. We analyzed the behavior of hMSCs cultured in the Michael network and incubated in growth media, with or without the respective TCO species, by fluorescence/immunofluorescence and gene analyses. The modular approach allows facile manipulation of synthetic matrices to regulate cell behavior for successful engineering of functional tissues.

2. Experimental Section.

2.1. General Information.

High molecular weight sodium hyaluronan (520 kDa) were obtained from Sanofi Genzyme Corporation (Cambridge, MA) as a gift and low molecular weight sodium hyaluronan (5 kDa) was obtained from Lifecore Biomedical (Chaska, MN). Diisopropylethylamine (DIPEA), ethyl ether, tetrahydrofuran (THF), dimethylformamide (DMF), trifluoroacetic acid (TFA), hexane, dichloromethane (DCM), TRIzol and paraformaldehyde were obtained from Thermo Fisher Scientific (Waltham, MA). Methyltetrazine-amine HCl salt (Me-Ph-Tz) was obtained from Click Chemistry Tools (Scottsdale, AZ). Triisopropylsilane (TIPS) and *N*-(3-dimethylaminopropyl)-*N*-ethylcarbodiimide hydrochloride (EDCI) were obtained from Sigma-Aldrich (St. Louis, MO). For peptide synthesis, amino acids with 9-fluorenylmethoxycarbonyl (Fmoc) protection were obtained from Protein Technologies (Tucson, AZ), resins (Rink Amide) were purchased from EMD Millipore Corporation (Billerica, MA), and 2-(1H-benzotriazole-1-yl)-1,1,3,3-tetramethyluronium hexafluorophosphate (HBTU) was obtained from Advanced Automated Peptide Protein Technologies (Louisville, KY). Bovine serum albumin (BSA), DAPI and Alexa Fluor® 568 phalloidin were purchased from Jackson Immuno Research, Millipore and Life Technologies, respectively. For immunofluorescence, the primary anti-integrin β1 antibody (mouse monoclonal, 12G10) and Alexa Fluor® 488-conjugated goat anti-mouse IgG were purchased from Abcam (Cambridge, MA) and Life Technologies (Grand Island, NY), respectively. For gene analysis, QuantiTect reverse transcription kit was obtained from Qiagen (Valencia, CA), power SYBR green master mix was obtained from Invitrogen (Carlsbad, CA) and primers were purchased from Integrated DNA Technologies (Coralville, IA).

2.2. Synthesis of Hydrogel Precursors.

2.2.1. HA-SH.—HA-SH was synthesized by reacting 520 kDa HA with 3,3’-dithiobis-propanoic dihydrazide in the presence of EDCI in water at pH 4.75 under vigorous

mechanical stirring. Upon treatment with 1,4-dithiothreitol, the mixture was dialyzed and the product was lyophilized.[28–29] By ^{1}H NMR (Figure S1), the degree of modification was estimated as 65 mol%.

2.2.2. Random Copolymer Carrying Both Acrylate and Tetrazine Groups (POM-AT).—A random copolymer of oligo (ethylene glycol) methyl ether methacrylate (OEGMA) and *tert*-butyl methacrylate (*t*BMA) was produced following our reported procedure. After deprotection of the carboxylates, acrylate (AC) groups were installed to produce acrylated copolymer (POM-A). POM-A had a M_n of 32 kDa and ~16 mol% of the methacrylic acid (MAA) repeats were acrylated.[30] To introduce the tetrazine functionality (Figure S2A), POM-A (100 mg) was first dissolved in DI water (4 mL) with pH adjusted to ~7.8. Next, an aqueous solution of Me-Ph-Tz (14 mg/mL, pH ~7.8) was slowly added, and the solution was agitated at room temperature for 48 h. After 48-h dialysis (MWCO 10K) against DI water, the pink product with dual AC and Tz functionalities (POM-AT) was obtained as lyophilized solid. Yield: 82%; ^{1}H NMR (D_2O, δ, Figure S2B): 5.9-6.5 ppm (j, k, l, -C***H***=C***H***$_2$ of acrylate), 7.5–8.5 ppm (-C_6***H***$_4$- in Me-Ph-Tz).

2.2.3. HA-TCO.—For the synthesis of HA-TCO, hydrazide-functionalized, dioxolane-fused *trans*-cyclooctene (dTCO-hydrazide) was first prepared by the reaction of dTCO-nitrophenyl [20] with hydrazine. Typically, a DCM solution (10 mL) of dTCO-nitrophenyl carbonate (150 mg, 0.43 mmol) was added dropwise to a DCM solution (5 mL) containing hydrazine (NH_2NH_2•H_2O, (1.7 mmol) and triethylamine (1.7 mmol). After 3-min stirring at room temperature, the mixture was diluted with 20 mL DCM before being washed with excess H_2O three times. After additional wash with $NaHCO_3$/H_2O, the organic DCM layer was collected and the oily product dTCO-hydrazide was obtained after drying (over Na_2SO_4), filtration and rotary evaporation. Yield: 85%; ^{1}H NMR ($CDCl_3$, δ, Figure S3Bi): 5.6–5.7 (m, 1H), 5.5–5.7 (m, 1H), 4.9 (t, 1H, J 3.0), 3.9–4.0 (m, 2H), 3.6–3.7 (m, 2H), 2.3–2.4 (m, 1H), 2.2–2.3(m, 1H), 2.1–2.2 (m, 1H), 1.7–1.9 (m, 2H), 1.6–1.7 (m, 2H), 1.5–1.6 (m, 1H).

HA-TCO was then prepared following the synthetic route shown in Figure S3A. Briefly, to an aqueous solution of HA (5 kDa, 60 mg in 12 mL water) at pH 4.75 was added 42 mg EDCI. Subsequently, 0.22 mmol dTCO-hydrazide in 1 mL DMSO/H_2O (1/1, v/v) was added and the solution was stirred at ambient temperature for 3 h. With pH adjusted to 8.5, the mixture was dialyzed against DI water (MWCO 1K) for 72 h. A white solid was obtained after freeze-drying. Yield: 88%; ^{1}H NMR (D_2O, δ, Figure S3Bii): ~1.9 ppm (a, -COC***H***$_3$ in HA), 5.5–5.7 ppm (b, c, -C***H***=C***H***$_2$ of TCO), 5.0 ppm (d, -OC***H***O- of TCO).

2.2.4. Peptides

GIW-bisAM: MMP-degradable peptide (Figure S4A) with a sequence of K_{mtt}RDGPQGIWGQDRK_{mtt}, where K_{mtt} is methyltrityl-protected lysine, were prepared on a PS3 peptide synthesizer (Protein Technologies) using the Rink Amide resin. After the addition of the last amino acid, resins were treated with acetic anhydride (5 mL, 20% in DMF) in the presence of 300 μL of DIPEA for 20 min. The resin was shaken in 10 mL TFA/DCM (3/97, *v/v*) for 3 min three times to deprotect the lysine amines. Subsequently,

acrylic acid (172 μL, 2.5 mmol), HBTU (379 mg, 1.0 mmol) and 300 μL of DIPEA were successively added, and the reaction was maintained at ambient temperature for 30 min. The acrylic acid reaction was repeated a second time to ensure efficient coupling. After a DMF wash, the peptide was cleaved and deprotected in a mixture of TFA/H_2O/TIPS (95/2.5/2.5, *v/v*) for 3 h. The crude peptide, GIW-bisAM, with the C-terminus amidated, was collected after precipitation in cold ether. The product was purified by reverse-phase high-performance liquid chromatography (HPLC) using Waters preparative HPLC and the peptide purity was confirmed using a Shimadzu HPLC.[30] Peptide elution was monitored by UV absorbance at 214 nm (amide bond, Figure S4B) and 280 nm (tryptophan residue, Figure S4C). The molecular weight (Figure S4D) of the purified peptide was analyzed by electrospray ionization mass spectrometry (ESI-MS, Thermo LCQ LC-MS system with ion trap mass analyzer, San Jose, CA). MS (m/z): $[M+3H]^{3+}$, calculated: 597.7, Found: 597.7; $[M+2H]^{2+}$, calculated: 896.0, Found: 896.0.

RGD-TCO and RGD-AM: Prior to TCO or acrylate conjugation, RGD peptide with a sequence of GKGYGRGDSPG or KGGGRGDSPG (Figure S5) was synthesized similarly as described above. The cleaved product, with C-amidated and N-acetylated, was allowed to react with nitrophenyl carbonate-derived sTCO in anhydrous DMF to install TCO through the lysine amine. After HPLC purification, the product was analyzed by ESI-MS, as reported in our previous publication.[23] Alternatively, the RGD peptide was modified with acrylic acid on resin to install AM, followed by acid cleavage and HPLC purification, similar to that described above for GIW-bisAM. MS (m/z): $[M+H]^{+}$, calculated 982.0; Found 982.5.

2.3. Synthesis and Characterization of HA/POM Hydrogels.

2.3.1. Hydrogel Synthesis.—Aqueous solutions of HA-SH (20 mg/mL) and POM-AT (40 mg/mL) were prepared at pH 7.9 using PBS and 1 M NaOH. The components were then mixed at 1.5/1 (mol/mol) thiol to acrylate ratio. To render the Michael network protease degradable, GIW-bisAM (0.5 mM) was dissolved in the POM-AT solution. The solution was maintained at 37 °C for 2 h to afford a viscoelastic solid. Next, tetrazine-TCO ligation was employed to alter the gel properties. Specifically, hydrogels established by Michael addition were introduced to an aqueous bath containing HA-TCO (0.7 mM) or RGD-TCO (2 mM), and gels were maintained in the respective bath for up to 24 h.[21] Hydrogel homogeneity was confirmed by UV-vis spectroscopy and confocal microscopy (Figure S6). Enzymatic degradation of Michael gels containing GIW crosslinks was analyzed gravimetrically (Figure S7). The disappearance of the pink tetrazine chromophore (Figure S8) indicates the completion of the reaction. Hydrogel swelling and sol fraction were measured in triplicate following our established procedure.[31]

2.3.2. Mechanical Properties.—The mechanical properties of HA/POM gels were analyzed by oscillatory rheometry using an AR-G2 rheometer (TA Instruments, New Castle, DE). To characterize the primary Michael network, the HA/POM solution was introduced on the bottom plate (8 mm) immediately upon mixing, and time sweep was conducted following our reported procedure.[31] To monitor the viscoelastic property of secondary tetrazine network during the tetrazine-TCO reaction, a pre-formed Michael gel was mounted inside a plastic cylinder immobilized on the bottom plate. After the top plate was lowered to

the gel surface, time sweep was initiated. Then, HA-TCO solution was added in the cylinder during the experiment. Separately, Michael gels were produced in cell culture inserts. After 6 h incubation at 37 °C, 200 μL of HA-TCO (0.7 mM) or RGD-TCO (2 mM) solution was overlaid on top of the hydrogel. The TCO solution was removed 24 h later, and the hydrogel was mounted on the bottom plate. Time sweep experiments were conducted at 1 Hz at 1% strain. All measurements were performed at 37 °C in triplicate. The reported values for storage (G') and loss (G") moduli represent the average ± standard deviation (SD).

2.4. Modulation of Stem Cell Behavior.

2.4.1. Fabrication of Cellular Constructs.—

Human bone marrow derived mesenchymal stem cells (hMSCs) were maintained in a MSCBM media supplemented with MSCGM SingleQuot Kit (Lonza, Allendale, NJ) at 37 °C with 5% CO_2. Media was refreshed every other day. Upon reaching 90% confluence, cells were detached from the plate using 0.05% (w/v) trypsin containing ethylenediaminetetraacetic acid (EDTA·4Na). For cell encapsulation, hMSCs were dispersed in the solution of HA-SH (20 mg/mL). After the addition of POM-AT (40 mg/mL), NaOH (1 M) was added to adjust the pH to 7.9. The gel mixture containing 1×10^6 cells per mL was aliquoted to individual inserts in a 24-well plate. After 30-min incubation at 37 °C, media was introduced to each well and insert to submerge the cellular construct. Two or six days post encapsulation, 200 μL of HA-TCO (0.7 mM) or RGD-TCO (2 mM) dissolved in media was introduced to the insert to allow interfacial bioorthogonal reaction to occur during cell culture. Twenty-four hours later, TCO-conditioned media was changed to the normal media. Control experiments were carried out using RGD-AM, instead of RGD-TCO. Media was refreshed every other day and the constructs were inspected by a Nikon microscope (Eclipse Ti-E, Tokyo, Japan).

2.4.2. Cell Viability.—

After 9 days of culture, cell-laden hydrogels were treated with calcein-AM (1:1000 dilution) and ethidium homodimer-1 (1:500 dilution) for 20 min to stain for live and dead cells, respectively.[30] Confocal images were recorded from three biological replicas using Zeiss LSM 710 with a 10x objective. Maximum intensity projections were produced by flattening ~300-μm thick z-stacks using Zeiss's Zen software. Using ImageJ, cell viability was quantified as the percentage of live cells out of the sum of live and dead cells.

2.4.3. Cell Morphology.—

Following our reported procedures,[30] cultures were terminated on day 9, and constructs were fixed with paraformaldehyde. Subsequently, cells were permeabilized with Triton X-100 and samples were blocked with BSA. F-actin was stained using Alexa Fluor® 568-labeled phalloidin and cell nuclei were counter stained with DAPI. Selected samples were co-stained for integrin-β1 using monoclonal mouse anti-intergrin β1 and Fluor® 488-conjugated goat anti-mouse IgG. Images were acquired using a Zeiss LSM 710 confocal microscope and maximum intensity projections were produced from 200–300 μm thick z-stacks. Images were recorded from three biological replica and the percentage of cells undergoing morphological changes, as compared to the controls, was analyzed by counting elongated and round cells in each image.

2.4.4. Gene Expression.—For gene analysis, cultures were terminated on day 9 and constructs were immediately frozen at −80 °C. After TRIzol digestion, the extracted RNA was reverse-transcribed to cDNA using Qiagen's QuantiTect kit. Next, SYBR green master mix (2x, 10 mL) was combined with the cDNA templates (4 ng) and the primers (400 nM) and real-time quantitative polymerase chain reaction (PCR) reaction was carried out using an ABI 7300 real-time PCR system. Glyceraldehyde 3-phosphate dehydrogenase (GAPDH) was used as a reference target and data were normalized and processed using commercially available qbase+ software (Biogazelle, Zwijnaarde, Belgium). A total of three biological repeats, each with at least 5 technical repeats, were analyzed for each gel composition. Results are presented as the mean ± standard error of the mean (SEM).

2.5. Statistical Analysis.

Data sets were compared using one-way analysis of variance (ANOVA) and a p value less than 0.05 was considered significant.

3. Results and Discussion

3.1. Characterization of Synthetic ECM.

3.1.1. Synthesis of Hydrogel Precursors.—Hydrogel precursors (Figure 1B) for the construction of the dynamic matrix were synthesized following standard chemical transformations. HA,[32] a natural non-sulphated glycosaminoglycan abundant in connective tissue ECM, was chemically modified with a latent disulfide compound to produce HA-SH with an estimated 65 mol% thiolation (Figure S1). HA with a number average molecular weight (M_n) of ~520 kDa was used to ensure the connectivity of the primary Michael network. A random copolymer of oligomeric (ethylene glycol) methacrylate (OEGMA) and methacrylic acid (MAA) with M_n of ~32 kDa, synthesized by living radical polymerization followed by acid hydrolysis,[30] was used as a carrier for both acrylate and tetrazine functionalities. Partial esterification of methacrylic acid repeats with hydroxyethyl acrylate installed the acrylate functionality, and subsequent conjugate addition reaction of methyltetrazine amine yielded a polymer (POM-AT) with both with 6 ± 2% acrylate and 10 ± 2% tetrazine functionalities, respectively. The successful conjugation of tetrazine was confirmed by UV-vis spectroscopy and ^{1}H NMR (Figure S2). Integration of vinyl protons and the methyl protons in OEGMA suggested that 10 ± 2 mol% of MAA repeats were Tz modified, while 6 ± 2 mol% were acrylated. Each POM chain carried approximately 11 to 13 Tz and 7 to 8 acrylate groups. In addition, UV-vis spectroscopy confirmed the conjugation of Tz, as evidenced by the absorbance maximum at 260 nm[33] from Me-Ph-Tz (Figure S2C). Tz functionality was calculated using Beer-Lambert Law and taking into consideration for the molar extinction coefficient of Me-Ph-Tz, determined using an aqueous solution of Me-Ph-Tz at concentrations of 0.007 to 0.06 mM. In agreement with the ^{1}H NMR result, ~8 mol% of the MAA repeats were conjugated with Tz.

In order to tune the matrix stiffness during 3D cell culture employing tetrazine-TCO ligation, HA was modified by a dioxolane-fused TCO,[20] which was chosen for its high reactivity and improved hydrophilicity (Figure S3). Low molecular weight HA (5 kDa) was used to ensure rapid diffusion of HA-TCO through the network. By ^{1}H NMR integration

(Figure S3Bii), comparing the acetal and alkene resonances from TCO to the acetamido resonances from *N*-acetyl-D-glucosamine indicated 28 mol% TCO incorporation (3-4 TCO groups per HA chain).

Degradability of the matrix by cell-secreted proteases is desirable to maintain proper cell functions in 3D.[34–36] Accordingly, matrix metalloproteinase (MMP)-cleavable peptide with a sequence of GPQGIWGQ (abbreviated as GIW) was incorporated in the primary network. Charged amino acid residues were added to improve peptide solubility in aqueous media and to enable functionalization with acrylic acid (Figure S4A). To conjugate integrin binding peptide during 3D cell culture through dangling tetrazines, a highly reactive TCO-dienophile[18] was conjugated to GKGYGRGDSPG peptide through the lysine amine (Figure S5). Our previous investigation showed that such derivation does not compromise the ability of cells to bind the RGD peptide.[23] An acrylamide-functionalized RGD (Figure S5) was synthesized as a control.

3.1.2. Fabrication of Hydrogel Networks.—The primary network was established via Michael addition by mixing HA-SH and POM-AT at pH ~7.9 with a slight excess of thiols relative to acrylate groups. The resultant hydrogel displaying dangling tetrazine groups had a swelling ratio of 18.1 ± 1.6 and a sol fraction of 30.9 ± 8.2%. Incorporation of thiol-reactive, MMP-degradable crosslinker, GIW-bisAM, in the Michael network at 0.5 mM gave rise to gels with a lower swelling ratio (13.4 ± 0.7) and sol fraction (19.8 ± 1.4%). Characterization of the primary Michael network by oscillatory shear rheology (Figure 2A, B) revealed that gelation occurs immediately upon mixing of HA-SH and POM-AT. The shear elastic modulus (G') continued to rise gradually through the slow thiol/acrylate reaction.[29] A plateau G' of 180 ± 42 Pa was obtained 2 and 3 h after mixing for gels with or without the GIW crosslinker, respectively.

The homogeneity of the primary Michael network was inspected spectroscopically and microscopically (Figure S6). Neither HA-SH nor POM-AT alone exhibited turbidity at the final hydrogel concentrations, as assessed by low absorbance at 600 nm.[37] No turbidity was observed from the gel mixture either. In addition, POM-AT alone and the HA-SH/POM-AT mixture exhibit a similar absorbance for the tetrazine chromophore at 525 nm.[33, 38] For confocal imaging, POM in the primary network was fluorescently labeled via interfacial tetrazine ligation using Cy3-TCO. The hydrogel was devoid of any phase-separated microstructures[39] and displayed Cy3 signal homogenously throughout the samples (Figure S6B). Collectively, HA-SH and POM-AT was homogeneously mixed as a single phase under gelation conditions. When incubated in PBS containing 100 U/mL Collagenase type IV, a gradual mass loss over time was observed for GIW-containing gels, with an ultimate mass loss of 16 ± 2% by day 12 (Figure S7). By contrast, gels incubated in enzyme free media were intact, suggesting minimal hydrolytic degradation within the period of the experiment. The moderate level of collagenase-mediated degradation reflects the low density of MMP-cleavable linkages incorporated in the primary network; approximately 1 out of 11 crosslinks were MMP-degradable. Unless otherwise noted, MMP-degradable gels were used in subsequent studies.

It was possible to stiffen the primary network of the hydrogel through the reaction with HA-TCO, which forms crosslinks with Tz groups dangling from the primary network. Time sweep experiments (Figure 2C) revealed that upon introduction of the hydrogel disk to the HA-TCO bath, the G' value of the hydrogel increased accordingly. The successful installation of the tetrazine network was further confirmed by the disappearance of tetrazine chromophore (pink color) in 4 h, as shown in Figure S8. The Michael gel, prepared as a soft and pliable disk, sank to bottom of a vial when transferred to HA-TCO (0.7 mM) solution. Within 15 min, the outer shell of the hydrogel disk became colorless, and the disk became buoyant, presumably due to the release of N_2 during tetrazine ligation. Over the course of the next 4 h, the non-crosslinked core of the hydrogel disk disappeared as HA-TCO crosslinked the gel from the "outside in".[21]

To assess the crosslinking kinetics and the evolution of gel properties under 3D cell culture conditions, the Michael gels were prepared in a cell culture insert and a solution of HA-TCO was overlaid on top of the gel disk to install the secondary network (Figure 3Ai). In this experiment, diffusion is one-dimensional and can be monitored by the disappearance of the pink color at the diffusion interface. After incubation time for >10 h, the pink color had disappeared completely, indicating that the complete consumption of the pendant tetrazines. Twenty-four hours post treatment with HA-TCO, the hydrogel exhibited a G′ of 520 ± 80 Pa (Figure 3B), which is significantly higher than that of the initially formed Michael gel (180 ± 42 Pa). The stiffening of the matrix is consistent with the formation of the new crosslinks in the network by tetrazine ligation. The tanδ (G"/G') value for both networks remained low (<0.05), confirming the elastic nature of the networks.

Next, we explored the utility of tetrazine ligation for the covalent tagging of cell-adhesive peptides with the tetrazine substituents on the primary network. Here, a solution of RGD-TCO was overlaid on top of the Michael gel (Figure 3Aii). Again, the pink color disappeared as RGD-TCO diffused through the interface, forming a colorless hydrogel as the interface advanced. After 6 h, the pink color had completely disappeared, consistent with complete modification of the tetrazine side chains. Incubation with monofunctional RGD-TCO led to the installation of dangling peptide chains that serve as non-elastic network defects without affecting the free diffusion of RGD-TCO. Thus, RGD tagging did not significantly alter the mechanical properties of the network, and the resultant gel maintained a G' value of 160 ± 60 Pa (Figure 3C). Compared to the HA-TCO treatment, a shorter incubation time is required for the pink color to disappear for RGD-TCO modified gels because of a slower diffusion of HA-TCO through the reinforced hydrogel network.

3.2. *In Situ* Modulation of Stem Cell Behavior.

The tunable synthetic ECM was utilized as a model platform to investigate cell behaviors via a user-directed interfacial bioorthogonal reaction during 3D cell culture. This design mimics the dynamic nature of the native ECM during embryogenesis, tumorigenesis and tissue repair. Tissue stiffening and the enhancement in matrix adhesivity are the hallmarks of these biological events.[40] hMSCs were employed in this work because they can be easily expanded in culture and differentiated into specific cell types in response to the changes in stem cell niche under the influence of potent inducers.[41–42] The ability to maintain stemness

and induce differentiation has significant implications in wound healing for tissue engineering applications.[43–44]

3.2.1. ***Cell Morphology.—***In our study, cells were encapsulated in the primary Michael network and two days later, HA-TCO was used to increase the matrix stiffness, while RGD-TCO was used to tag the matrix with a cell adhesive motif without changing the matrix stiffness. Live/dead staining (Figure 4A) revealed that the cells were highly viable after 9 days of culture. (cell viability ~95%, Figure 4B), confirming the cytocompatibility of the hydrogel formulations. First, we investigated the effect of matrix stiffening on hMSCs during 3D culture (Figure 5). Cultures were maintained in hMSC growth media and monitored using a fluorescence microscope in bright field mode up to 9 days (Figure 5A). Cells in MMP-degradable Michael gels with or without HA-TCO treatment remained mostly rounded during early days of culture. By day 9, however, 22 ± 4% cells in control gels and 28 ± 3% cells in HA-TCO gels ($p>0.05$) had developed thin hair-like projections and were stellate-shaped (Figure 5A). A few spindle shaped cells were present close to the bottom of the gels.

Fluorescent staining and confocal imaging of day 9 cultures (Figure 5B) revealed that the majority of hMSCs were homogeneously distributed in both control and HA-TCO gels as single, rounded cells with distinct cortical actin. A few cells developed small actin-rich, filopodia-like processes (Figure 5B, inserts). Nevertheless, the morphological changes were more pronounced in HA-TCO treated gels than in the untreated controls. If the primary Michael gels lacked the GIW crosslinks, network stiffening by HA-TCO on day 2 did not cause any detectable changes in cell morphology by day 9 (Figure S9A, B). Thus, cell-mediated matrix degradation is essential to promote for cell-matrix interactions.[45] Under the experimental conditions employed, hMSCs expressed integrin β-1 (ITGb1, Figure S9) and can potentially bind HA via CD44 and RHAMM[28] to elicit motility associated with dynamic cytoskeletal changes.[46] The ability of the network to retain ECM proteins secreted by the resident cells, although not detectable by immunofluorescence (data not shown), may also contribute to the development of cellular extensions. Collectively, tetrazine ligation-mediated stiffening of MMP-degradable Michael network enabled hMSCs to locally interact with the network through the development of small filopodia-like structures without significantly altering the overall cell morphology.

Next, we studied if temporally controlled bioorthogonal tagging could be used to modify the ECM and influence hMSC function. RGD tagging 2 days post encapsulation promoted significant cell spreading by day 5 (Figure 6A). Cells continued to spread and elongate along a single axis in 3D to establish an interconnected cellular mesh by day 9. Confocal microscopy revealed the development of polarized, elongated morphology with bundles of cytoskeleton stress fibers distributed throughout the entire cellular extensions (Figure 6B). Organization of actin monomer into stress fibers indicates active actin polymerization events leading to the development of load-bearing cell-matrix binding that is conducive to cell extension in 3D. In the absence of MMP-cleavable peptide substrate in the primary network, the addition of RGD-TCO on day 2 failed to induce hMSC spreading (Figure S9C) by day 9. Again, restricting hMSCs in a “covalent cage” that lacks macroscopic pores and are not susceptible to protease-mediated matrix remodeling prohibits the acquisition of normal

mesenchymal morphology. Introduction of the RGD signal 6 days post encapsulation also triggered significant cell spreading. By day 8, elongated cells with extended and interconnected cellular processes were abundant (Figure S10).

To ensure the observed cellular response was due to the covalent conjugation of the RGD signal, control experiments were performed using acrylamide-tagged RGD (RGD-AM) that does not participate in tetrazine ligation. RGD-AM, instead of unfunctionalized RGD, was used in the control experiment to ensure a similar hydrophobicity with RGD-TCO. Covalent tagging of RGD-AM to the Michael network is expected to be very inefficient because thiol/acrylate reaction is slow and free thiols can be readily oxidized to disulfide. Indeed, our results (Figure S11) show that hMSCs cultured in gels treated with RGD-AM were morphologically similar to those in control gels without any modification, in sharp contrast to the triggered cell spreading and extension seen in gels that were covalently modified with RGD through tetrazine ligation.

Under the experimental conditions employed, as soon as RGD-TCO comes in contact with the tetrazine groups dangling from the primary network, tetrazine ligation occurs at the gel-liquid interface and the reaction is complete instantaneously with close to 100% efficiency.[21] Blocking of cell surface integrin binding sites by soluble RGD-TCO prior to its immobilization on the network is unlikely as this TCO/Tz pair reacts with $k_2 > 10^5\ M^{-1}s^{-1}$. While the interfacial reaction is instantaneous, the complete consumption of tetrazine moieties takes 6 h owing to the unidirectional nature of the diffusion. Collectively, RGD tagging could be used to induce morphological changes in hMSCs by *in situ* modification of ECM.

3.2.2. Gene Expression.—qPCR analyses were performed to identify cellular responses to RGD tagging, in terms of expression levels of transcripts encoding important ECM proteins and putative differentiation markers (Figure 7). As seen in Figure 7B, RGD tagging significantly decreased ($p<0.05$) cellular expression of type III collagen (α3 chain, COL3A1, 1.38 ± 0.04-fold), type I collagen (α 1 chain, COL1A1, 1.28 ± 0.09-fold) and tenasin C (TNC, 1.40 ± 0.13-fold). Although not significant, the expression of fibronectin (FN) in RGD-TCO treated gels were 1.13 ± 0.12 lower than the blank controls. Conversely, the expression of MMP1 was significantly ($p<0.05$) increased (1.64 ± 0.27-fold). Expression levels of transcripts encoding fibroblastic (FSP-1: fibroblast specific protein-1)[47] and adipogenic (aP2: adipocyte protein 2)[48] phenotypes were comparable between the controls and the RGD-TCO treated samples. However, RGD tagging resulted in a significant ($p<0.05$) down regulation of chondrogenic[49] (AGN: aggrecan, 1.40 ± 0.10 fold), osteogenic[50] (ALP: alkaline phosphatase, 1.40 ± 0.09 fold) and myofibroblastic[51] (αSMA: alpha smooth muscle actin, 1.37 ± 0.15 fold) differentiation.

Our qPCR results revealed that the potential of classic osteoblastic, chondrogenic, adipogenic, or myofibroblastic differentiation was suppressed at the transcriptional level in RGD-TCO treated constructs as compared to the RGD-free controls. Considering TNC and COL1/3 as the broad fibroblastic hallmarks,[52–53] it is clear that RGD tagging also suppressed the fibroblastic commitment of hMSCs. Matrix metalloproteinases are commonly found to be upregulated during the wound healing response in hMSCs,[54] and

have been implicated in turnover of fibrotic tissue.[55–56] Upregulation of MMP1, along with downregulation of COL1A1, COL3A1, indicate that cells are moving towards a net catabolic state in the RGD-treated gels.

It is widely acknowledged that the manipulation of stem cell niches, particularly the incorporation of integrin binding motifs, is an effective approach to guide stem cell fate selection.[57] In most studies, hMSCs encapsulated in synthetic ECM were maintained for a longer time (>21 days) in specific differentiation media containing potent inductive factors.[58–59] Depending on the matrix compositions and culture conditions, RGD was reported to promote or inhibit chondrogenesis and osteogenesis.[60–63] In our case, cellular constructs were cultivated in the growth media for 7 days after the RGD signal was introduced. Even though MMP-degradable linker was present in both gels, only when RGD was introduced could cells actively degrade the matrix.

Collectively, RGD tagging did not promote specific lineage commitment, even though cells in these gels develop extensive cellular processes and adopted elongated cell morphology. It is well documented that cell shape determines cell function.[64–65] The fact that RGD tagging caused pronounced morphological changes in hMSCs without compromising their stemness implies that these cells would be more susceptible to lineage-specific differentiation when potent inductive signals are subsequently introduced. To this end, we are developing RNA sequencing and bioinformatics methods to gain a broad, global view of differential expressions and to identify specific signaling pathways that are activated. Once the gene targets are identified, protein-level analysis will be carried out to gain more in-depth understanding of hMSC differentiation. Establishing a biomimetic microenvironment that regulates cell morphology is a powerful strategy for controlling cell physiology, a first step towards the establishment of engineered tissues or tissue models.

4. Conclusion

In summary, we described a novel method for *in situ* tuning of the cellular microenvironment to alter the behaviors of hMSCs cultured in a 3D biomimetic matrix. While the slow Michael addition facilitated the 3D encapsulation of hMSCs, the fast tetrazine ligation enabled a time-delayed modification of the synthetic ECM. The key matrix component is a well-defined, random copolymer carrying both acrylate and tetrazine groups. The rapid, bioorthogonal Tz/TCO reaction enables straightforward adjustment of matrix properties to elicit corresponding cellular responses without negatively affecting normal cell functions. Specifically, tetrazine-ligation mediated tagging of integrin-binding RGD peptide to the MMP-degradable network significantly altered cell morphology, through the development of extensive F-actin rich structures. Our observation is in line with recent reports revealing that 3D cell migration is cell-type independent and can be regulated by extracellular cues.[66–68] Our synthetic matrices recapitulate key properties and functions of natural ECMs, allowing dynamic and systematic tuning of the cellular environment at a molecular level.

Supplementary Material

Refer to Web version on PubMed Central for supplementary material.

Acknowledgements:

This work was supported in part by National Institutes of Health (NIH, R01DC011377, R01DC014461 and R01DE022969), National Science Foundation (NSF, DMR 1506613) and Delaware Bioscience Center for Advanced Technology (DE CAT). KTD acknowledges W. L. Gore and Associates for the Gore Fellowship. ABZ acknowledges financial support by NSF IGERT Fellowship. Spectra were obtained with instrumentation supported by NIH grants (P20GM104316, P30GM110758, S10RR026962, S10OD016267) and NSF grants (CHE-0840401 and CHE-1229234). Microscopy access was supported by grants from the NIH-NIGMS (P20 GM103446), the NSF (IIA-1301765) and the State of Delaware. We appreciate Genzyme/Sonofi for providing research grade HA.

References

(1). Lee KY; Mooney DJ Hydrogels for Tissue Engineering. Chem. Rev 2001, 101, 1869–1880. [PubMed: 11710233]

(2). Seliktar D Designing Cell-Compatible Hydrogels for Biomedical Applications. Science 2012, 336, 1124–1128. [PubMed: 22654050]

(3). Kloxin AM; Kloxin CJ; Bowman CN; Anseth KS Mechanical Properties of Cellularly Responsive Hydrogels and Their Experimental Determination. Adv. Mater 2010, 22, 3484–3494. [PubMed: 20473984]

(4). Wade RJ; Burdick JA Engineering ECM Signals into Biomaterials. Mater. Today 2012, 15, 454–459.

(5). Wang H; Heilshorn SC Adaptable Hydrogel Networks with Reversible Linkages for Tissue Engineering. Adv. Mater 2015, 27, 3717–3736. [PubMed: 25989348]

(6). Rosales AM; Anseth KS The Design of Reversible Hydrogels to Capture Extracellular Matrix Dynamics. Nat. Rev. Mater 2016, 1, 15012. [PubMed: 29214058]

(7). Chen X; Dam MA; Ono K; Mal A; Shen H; Nutt SR; Sheran K; Wudl F A Thermally Re-endable Cross-Linked Polymeric Material. Science 2002, 295, 1698–1702. [PubMed: 11872836]

(8). Krogsgaard M; Behrens MA; Pedersen JS; Birkedal H Self-Healing Mussel-Inspired Multi-pH-Responsive Hydrogels. Biomacromolecules 2013, 14, 297–301.

(9). Adzima BJ; Kloxin CJ; Bowman CN Externally Triggered Healing of a Thermoreversible Covalent Network via Self-Limited Hysteresis Heating. Adv. Mater 2010, 22, 2784–2787. [PubMed: 20408134]

(10). Bowman CN; Kloxin CJ Covalent Adaptable Networks: Reversible Bond Structures Incorporated in Polymer Networks. Angew. Chem., Int. Edit 2012, 51, 4272–4274.

(11). Guvendiren M; Burdick JA Stiffening Hydrogels to Probe Short- and Long-Term Cellular Responses to Dynamic Mechanics. Nat. Commun 2012, 3, 792. [PubMed: 22531177]

(12). DeForest CA; Polizzotti BD; Anseth KS Sequential Click Reactions for Synthesizing and Patterning Three-Dimensional Cell Microenvironments. Nat. Mater 2009, 8, 659–664. [PubMed: 19543279]

(13). Williams CG; Malik AN; Kim TK; Manson PN; Elisseeff JH Variable Cytocompatibility of Six Cell Lines with Photoinitiators Used for Polymerizing Hydrogels and Cell Encapsulation. Biomaterials 2005, 26, 1211–1218. [PubMed: 15475050]

(14). Bryant SJ; Nuttelman CR; Anseth KS Cytocompatibility of UV and Visible Light Photoinitiating Systems on Cultured NIH/3T3 Fibroblasts In Vitro. J. Biomat. Sci., Polym. E 2000, 11, 439–457.

(15). Sletten EM; Bertozzi CR Bioorthogonal Chemistry: Fishing for Selectivity in a Sea of Functionality. Angew. Chem., Int. Edit 2009, 48, 6974–6998.

(16). Dommerholt J; van Rooijen O; Borrmann A; Guerra CF; Bickelhaupt FM; van Delft FL Highly Accelerated Inverse Electron-Demand Cycloaddition of Electron-Deficient Azides with Aliphatic Cyclooctynes. Nat. Commun 2014, 5, 5378. [PubMed: 25382411]

(17). Blackman ML; Royzen M; Fox JM Tetrazine Ligation: Fast Bioconjugation Based on Inverse-Electron-Demand Diels-Alder Reactivity. J. Am. Chem. Soc 2008, 130, 13518–13519. [PubMed: 18798613]

(18). Taylor MT; Blackman ML; Dmitrenko O; Fox JM Design and Synthesis of Highly Reactive Dienophiles for the Tetrazine–Trans-Cyclooctene Ligation. J. Am. Chem. Soc 2011, 133, 9646–9649. [PubMed: 21599005]

(19). Selvaraj R; Fox JM Trans-Cyclooctene- A Stable, Voracious Dienophile for Bioorthogonal Labeling. Curr. Opin. Chem. Biol 2013, 17, 753–760. [PubMed: 23978373]

(20). Darko A; Wallace S; Dmitrenko O; Machovina MM; Mehl RA; Chin JW; Fox JM Conformationally Strained Trans-Cyclooctene with Improved Stability and Excellent Reactivity in Tetrazine Ligation. Chem. Sci 2014, 5, 3770–3776. [PubMed: 26113970]

(21). Zhang H; Dicker KT; Xu X; Jia X; Fox JM Interfacial Bioorthogonal Cross-Linking. ACS Macro. Lett 2014, 3, 727–731. [PubMed: 25177528]

(22). Liu S; Zhang H; Remy RA; Deng F; Mackay ME; Fox JM; Jia X Meter-Long Multiblock Copolymer Microfibers via Interfacial Bioorthogonal Polymerization. Adv. Mater 2015, 27, 2783–2790. [PubMed: 25824805]

(23). Zhang H; Trout WS; Liu S; Andrade GA; Hudson DA; Scinto SL; Dicker KT; Li Y; Lazouski N; Rosenthal J; Thorpe C; Jia X; Fox JM Rapid Bioorthogonal Chemistry Turn-on through Enzymatic or Long Wavelength Photocatalytic Activation of Tetrazine Ligation. J. Am. Chem. Soc 2016, 138, 5978–5983. [PubMed: 27078610]

(24). Liu S; Moore AC; Zerdoum AB; Zhang H; Scinto SL; Zhang H; Gong L; Burris DL; Rajasekaran AK; Fox JM; Jia X Cellular Interactions with Hydrogel Microfibers Synthesized via Interfacial Tetrazine Ligation. Biomaterials 2018, DOI: 10.1016/j.biomaterials.2018.06.042.

(25). Markisz JA; Gettler JD Quantitative Aspects of Base-Catalyzed Michael Addition: Mechanistic Study of Structural and Medium Effects on Rate. Can. J. Chem 1969, 47, 1965–1979.

(26). Cukierman E; Pankov R; Stevens DR; Yamada KM Taking Cell-Matrix Adhesions to the Third Dimension. Science 2001, 294, 1708–1712. [PubMed: 11721053]

(27). Lee J; Abdeen AA; Zhang D; Kilian KA Directing Stem Cell Fate on Hydrogel Substrates by Controlling Cell Geometry, Matrix Mechanics and Adhesion Ligand Composition. Biomaterials 2013, 34, 8140–8148. [PubMed: 23932245]

(28). Gurski LA; Xu X; Labrada LN; Nguyen NT; Xiao L; van Golen KL; Jia X; Farach-Carson MC Hyaluronan (HA) Interacting Proteins RHAMM and Hyaluronidase Impact Prostate Cancer Cell Behavior and Invadopodia Formation in 3D HA-Based Hydrogels. PLoS One 2012, 7, e50075. [PubMed: 23166824]

(29). Ozdemir T; Fowler EW; Liu S; Harrington DA; Witt RL; Farach-Carson MC; Pradhan-Bhatt S; Jia X Tuning Hydrogel Properties to Promote the Assembly of Salivary Gland Spheroids in 3D. ACS Biomater. Sci. Eng 2016, 2, 2217–2230. [PubMed: 27990487]

(30). Hao Y; Zerdoum AB; Stuffer AJ; Rajasekaran AK; Jia X Biomimetic Hydrogels Incorporating Polymeric Cell-Adhesive Peptide To Promote the 3D Assembly of Tumoroids. Biomacromolecules 2016, 17, 3750–3760. [PubMed: 27723964]

(31). Xu X; Gurski LA; Zhang C; Harrington DA; Farach-Carson MC; Jia X Recreating the Tumor Microenvironment in a Bilayer, Hyaluronic Acid Hydrogel Construct for the Growth of Prostate Cancer Spheroids. Biomaterials 2012, 33, 9049–9060. [PubMed: 22999468]

(32). Dicker KT; Gurski LA; Pradhan-Bhatt S; Witt RL; Farach-Carson MC; Jia X Hyaluronan: A Simple Polysaccharide with Diverse Biological Functions. Acta Biomater. 2014, 10, 1558–1570. [PubMed: 24361428]

(33). Devaraj NK; Weissleder R; Hilderbrand SA Tetrazine-Based Cycloadditions: Application to Pretargeted Live Cell Imaging. Bioconjugate Chem. 2008, 19, 2297–2299.

(34). Lutolf MP; Lauer-Fields JL; Schmoekel HG; Metters AT; Weber FE; Fields GB; Hubbell JA Synthetic Matrix Metalloproteinase-Sensitive Hydrogels for the Conduction of Tissue Regeneration: Engineering Cell-Invasion Characteristics. P. Natl. Acad. Sci. USA 2003, 100, 5413–5418.

(35). Galler KM; Aulisa L; Regan KR; D'Souza RN; Hartgerink JD Self-Assembling Multidomain Peptide Hydrogels: Designed Susceptibility to Enzymatic Cleavage Allows Enhanced Cell Migration and Spreading. J. Am. Chem. Soc 2010, 132, 3217–3223. [PubMed: 20158218]

(36). Kim J; Kim IS; Cho TH; Kim HC; Yoon SJ; Choi J; Park Y; Sun K; Hwang SJ In Vivo Evaluation of MMP Sensitive High-Molecular Weight HA-Based Hydrogels for Bone Tissue Engineering. J. Biomed. Mater. Res. A 2010, 95A, 673–681.

(37). Lau HK; Li L; Jurusik AK; Sabanayagam CR; Kiick KL Aqueous Liquid–Liquid Phase Separation of Resilin-Like Polypeptide/Polyethylene Glycol Solutions for the Formation of Microstructured Hydrogels. ACS Biomater. Sci. Eng 2017, 3, 757–766.

(38). Yong-Hua G; Fabien M; Rachel MR; Sophie B; Laurent G; Jie T; Pierre A; Gilles C Synthesis and Physical Chemistry of s-Tetrazines: Which Ones are Fluorescent and Why? Eur. J. Org. Chem 2009, 2009, 6121–6128.

(39). Abbadessa A; Landín M; Oude Blenke E; Hennink WE; Vermonden T Two-Component Thermosensitive Hydrogels: Phase Separation Affecting Rheological Behavior. Eur. Polym. J 2017, 92, 13–26.

(40). Müller P; Schier Alexander F. Extracellular Movement of Signaling Molecules. Dev. Cell 2011, 21, 145–158. [PubMed: 21763615]

(41). Pittenger MF; Mackay AM; Beck SC; Jaiswal RK; Douglas R; Mosca JD; Moorman MA; Simonetti DW; Craig S; Marshak DR Multilineage Potential of Adult Human Mesenchymal Stem Cells. Science 1999, 284, 143–147. [PubMed: 10102814]

(42). Baksh D; Song L; Tuan RS Adult Mesenchymal Stem Cells: Characterization, Differentiation, and Application in Cell and Gene Therapy. J. Cell. Mol. Med. 2004, 8, 301–316. [PubMed: 15491506]

(43). Chamberlain G; Fox J; Ashton B; Middleton J Concise Review: Mesenchymal Stem Cells: Their Phenotype, Differentiation Capacity, Immunological Features, and Potential for Homing. STEM CELLS 2007, 25, 2739–2749. [PubMed: 17656645]

(44). Caplan AI Adult Mesenchymal Stem Cells for Tissue Engineering versus Regenerative Medicine. J. Cell. Physiol. 2007, 213, 341–347. [PubMed: 17620285]

(45). Khetan S; Guvendiren M; Legant WR; Cohen DM; Chen CS; Burdick JA Degradation-Mediated Cellular Traction Directs Stem Cell Fate in Covalently Crosslinked Three-Dimensional Hydrogels. Nat. Mater 2013, 12, 458–465. [PubMed: 23524375]

(46). Turley EA; Noble PW; Bourguignon LYW Signaling Properties of Hyaluronan Receptors. J. Biol. Chem 2002, 277, 4589–4592. [PubMed: 11717317]

(47). Strutz F; Okada H; Lo CW; Danoff T; Carone RL; Tomaszewski JE; Neilson EG Identification and Characterization of a Fibroblast Marker: FSP1. J. Cell Biol 1995, 130, 393–405. [PubMed: 7615639]

(48). Distel RJ; Ro H-S; Rosen BS; Groves DL; Spiegelman BM Nucleoprotein Complexes that Regulate Gene Expression in Adipocyte Differentiation: Direct Participation of c-fos. Cell 1987, 49, 835–844. [PubMed: 3555845]

(49). Barry F; Boynton RE; Liu B; Murphy JM Chondrogenic Differentiation of Mesenchymal Stem Cells from Bone Marrow: Differentiation-Dependent Gene Expression of Matrix Components. Exp. Cell Res 2001, 268, 189–200. [PubMed: 11478845]

(50). Siffert RS The Role of Alkaline Phosphatase in Osteogenesis *J. Exp. Med.* 1951, 93, 415–426. [PubMed: 14832392]

(51). Desmoulière A; Geinoz A; Gabbiani F; Gabbiani G Transforming Growth Factor-Beta 1 Induces Alpha-Smooth Muscle Actin Expression in Granulation Tissue Myofibroblasts and in Quiescent and Growing Cultured Fibroblasts. J. Cell Biol. 1993, 122, 103–111. [PubMed: 8314838]

(52). Tong Z; Sant S; Khademhosseini A; Jia X Controlling the Fibroblastic Differentiation of Mesenchymal Stem Cells Via the Combination of Fibrous Scaffolds and Connective Tissue Growth Factor. *Tissue Eng. Part A* 2011, 17, 2773–2785. [PubMed: 21689062]

(53). Lee CH; Shah B; Moioli EK; Mao JJ CTGF Directs Fibroblast Differentiation from Human Mesenchymal Stem/Stromal Cells and Defines Connective Tissue Healing in a Rodent Injury Model. J. Clin. Invest. 2010, 120, 3340–3349. [PubMed: 20679726]

(54). Jackson WM; Nesti LJ; Tuan RS Concise Review: Clinical Translation of Wound Healing Therapies Based on Mesenchymal Stem Cells. STEM CELLS Transl. Med 2012, 1, 44–50. [PubMed: 23197639]

(55). Fuja TJ; Probst-Fuja MN; Titze IR Changes in Expression of Extracellular Matrix Genes, Fibrogenic Factors, and Actin Cytoskeletal Organization in Retinol Treated and Untreated Vocal Fold Stellate Cells. Matrix Biol. 2006, 25, 59–67. [PubMed: 16253491]

(56). Kutty JK; Webb K Tissue Engineering Therapies for the Vocal Fold Lamina Propria. Tissue Eng. Part B: Rev. 2009, 15, 249–262. [PubMed: 19338432]

(57). Brizzi MF; Tarone G; Defilippi P Extracellular Matrix, Integrins, and Growth Factors as Tailors of the Stem Cell Niche. Curr. Opin. Cell Biol. 2012, 24, 645–651. [PubMed: 22898530]

(58). Li W-J; Tuli R; Huang X; Laquerriere P; Tuan RS Multilineage Differentiation of Human Mesenchymal Stem Cells in A Three-Dimensional Nanofibrous Scaffold. Biomaterials 2005, 26, 5158–5166. [PubMed: 15792543]

(59). Liu S; Tay LM; Anggara R; Chuah YJ; Kang Y Long-Term Tracking Mesenchymal Stem Cell Differentiation with Photostable Fluorescent Nanoparticles. ACS Appl. Mater. Interfaces 2016, 8, 11925–11933. [PubMed: 27124820]

(60). Yang F; Williams CG; Wang D.-a.; Lee H; Manson PN; Elisseeff J The Effect of Incorporating RGD Adhesive Peptide in Polyethylene Glycol Diacrylate Hydrogel on Osteogenesis of Bone Marrow Stromal Cells. Biomaterials 2005, 26, 5991–5998. [PubMed: 15878198]

(61). Steinmetz NJ; Bryant SJ The Effects of Intermittent Dynamic Loading on Chondrogenic and Osteogenic Differentiation of Human Marrow Stromal Cells Encapsulated in RGD-Modified Poly(Ethylene Glycol) Hydrogels. Acta Biomater. 2011, 7, 3829–3840. [PubMed: 21742067]

(62). Connelly JT; García AJ; Levenston ME Inhibition of in Vitro Chondrogenesis in RGD-Modified Three-Dimensional Alginate Gels. Biomaterials 2007, 28, 1071–1083. [PubMed: 17123602]

(63). Connelly JT; Petrie TA; García AJ; Levenston ME Fibronectin- and Collagen-Mimetic Ligands Regulate BMSC Chondrogenesis in 3D Hydrogels. Eur. Cells Mater. 2011, 22, 168–177.

(64). Guilak F; Cohen DM; Estes BT; Gimble JM; Liedtke W; Chen CS Control of Stem Cell Fate by Physical Interactions with the Extracellular Matrix. Cell Stem Cell 2009, 5, 17–26. [PubMed: 19570510]

(65). von Erlach TC; Bertazzo S; Wozniak MA; Horejs C-M; Maynard SA; Attwood S; Robinson BK; Autefage H; Kallepitis C; del Río Hernández A; Chen CS; Goldoni S; Stevens MM Cell-Geometry-Dependent Changes in Plasma Membrane Order Direct Stem Cell Signalling and Fate. Nat. Mater. 2018, 17, 237–242. [PubMed: 29434303]

(66). Charras G; Sahai E Physical Influences of the Extracellular Environment on Cell Migration. Nat. Rev. Mol. Cell Biol. 2014, 15, 813–824. [PubMed: 25355506]

(67). Chaudhuri O; Gu L; Klumpers D; Darnell M; Bencherif SA; Weaver JC; Huebsch N; Lee H.-p.; Lippens E; Duda GN; Mooney DJ Hydrogels with Tunable Stress Relaxation Regulate Stem Cell Fate and Activity. Nat. Mater. 2016, 15, 326–334. [PubMed: 26618884]

(68). Mabry KM; Schroeder ME; Payne SZ; Anseth KS Three-Dimensional High-Throughput Cell Encapsulation Platform to Study Changes in Cell-Matrix Interactions. ACS Appl. Mater. Interfaces 2016, 8, 21914–21922. [PubMed: 27050338]

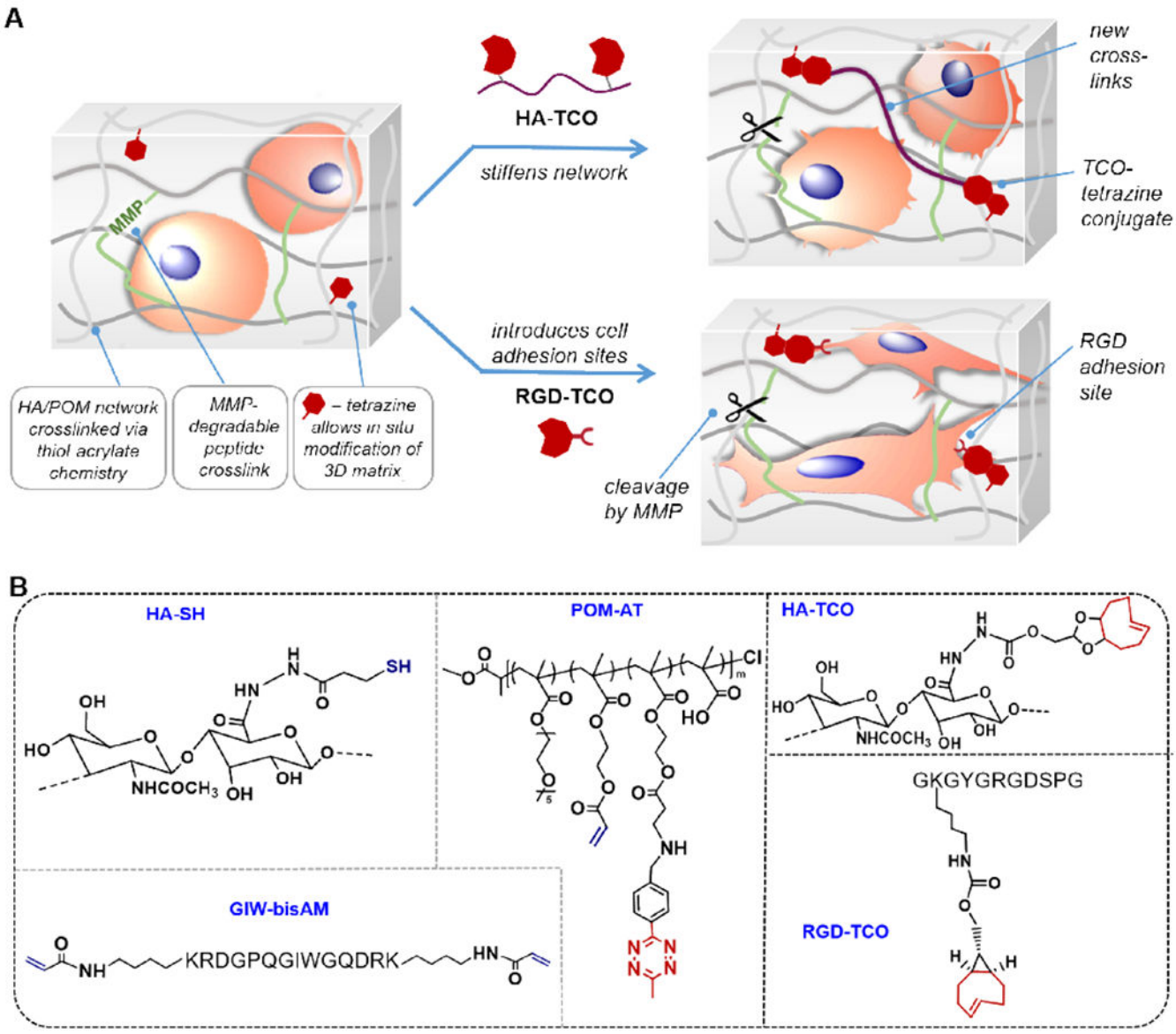

Figure 1.

Establishment and modification of 3D cultures using two independent bioconjugation reactions. hMSCs were encapsulated in the primary network using a slow thiol-acrylate reaction. During culture, tetrazine ligation was used to modify the existing network through a rapid, diffusion controlled reaction at the gel-liquid interface. (A): Schematic depiction of the evolution of the network properties and the corresponding cellular responses. (B): Structures of hydrogel building blocks carrying thiol, acrylate/acrylamide, tetrazine and TCO groups.

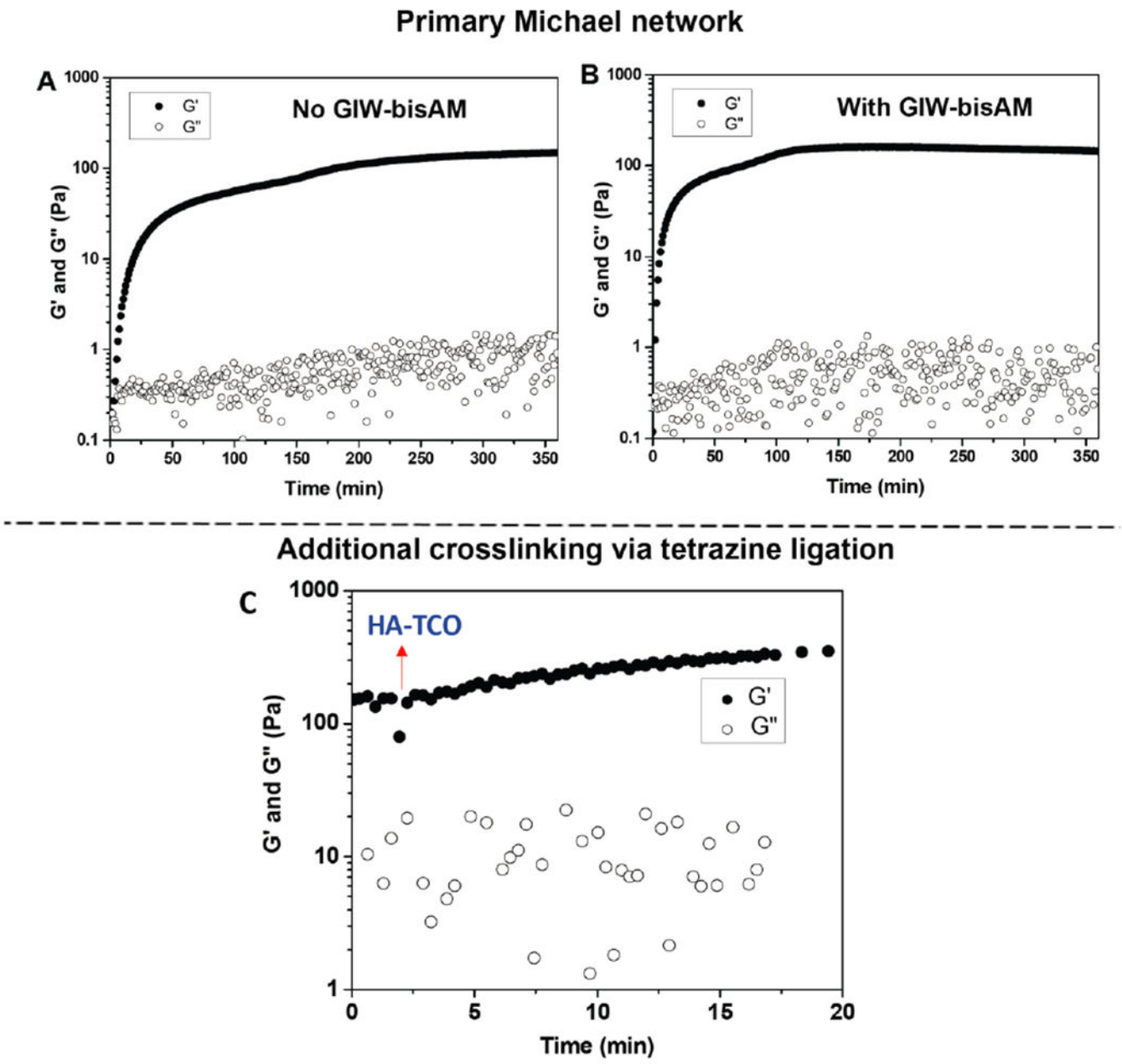

Figure 2.

Establishment of the primary Michael network and the introduction of additional crosslinks via tetrazine ligation, as assessed by oscillatory rheometry. (A, B): Time sweep experiments conducted on HA/POM gels established via thiol/acrylate reaction with or without MMP-degradable GIW-bisAM crosslinker. Samples were loaded on the plate immediately after the hydrogel precursors were mixed. (C): Stiffening of the primary MMP-degradable network through tetrazine ligation via a diffusion-controlled interfacial crosslinking using HA-TCO. At ~2 min, HA-TCO (0.7 mM) was added around the preformed gel on the plate and G′/G” values were monitored for 20 min.

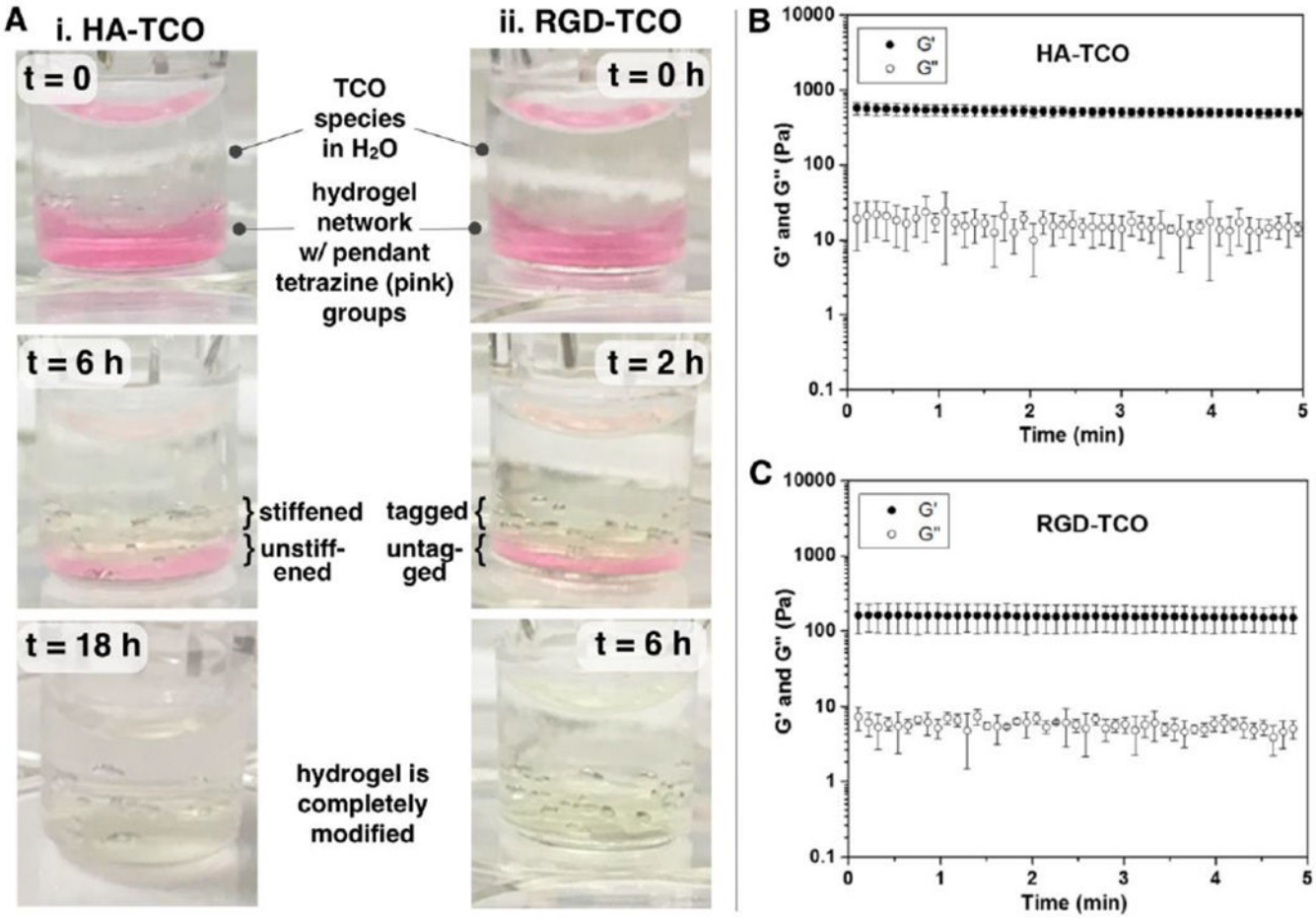

Figure 3.

Tetrazine ligation-mediated modification of the primary Michael gel under 3D cell culture conditions. Gels were prepared in cell culture inserts and the respective TCO solution was added on top of the gel disks. The TCO molecules diffused into the gel disk to introduce further crosslinking or to conjugate the cell adhesive peptide. The disappearance of tetrazine chromophore (A) indicated the consumption of tetrazines in the primary network. Twenty-four hours later, gels were collected for rheological analysis (B, C).

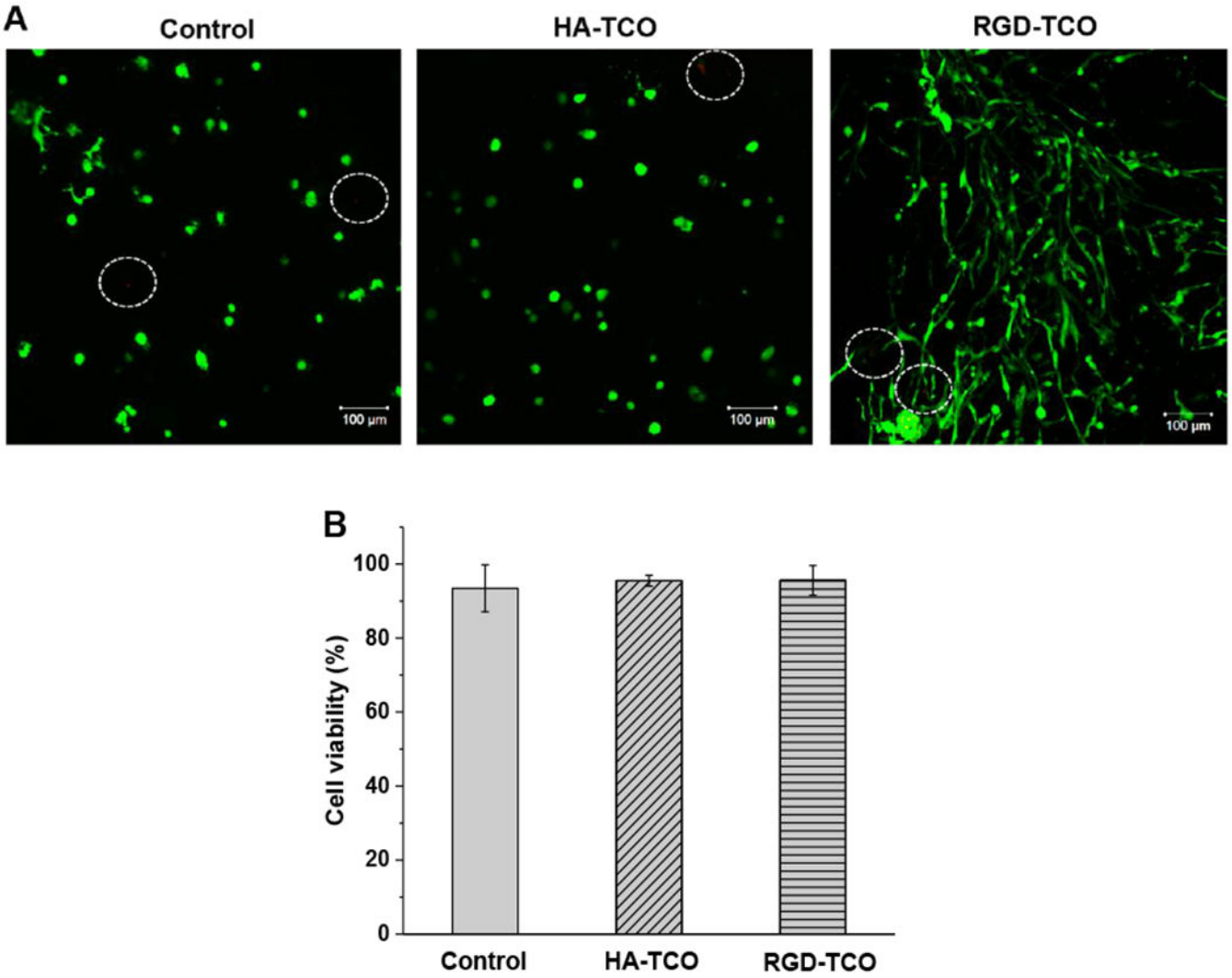

Figure 4:

Characterization of 3D cultures by live/dead staining. (A): Confocal images of hMSCs stained with calcein AM (live cells, green) and ethidium homodimer-1 (dead cells, red) after 9 days of culture in the primary, MMP-degradable Michael network (control) or with HA-TCO or RGD-TCO treatment on day 2. White circles highlight dead cells. (B): Quantification of cell viability based on live/dead assay using ImageJ. No statistical significance ($p>0.05$) was observed between the control, RGD-TCO or HA-TCO treated samples.

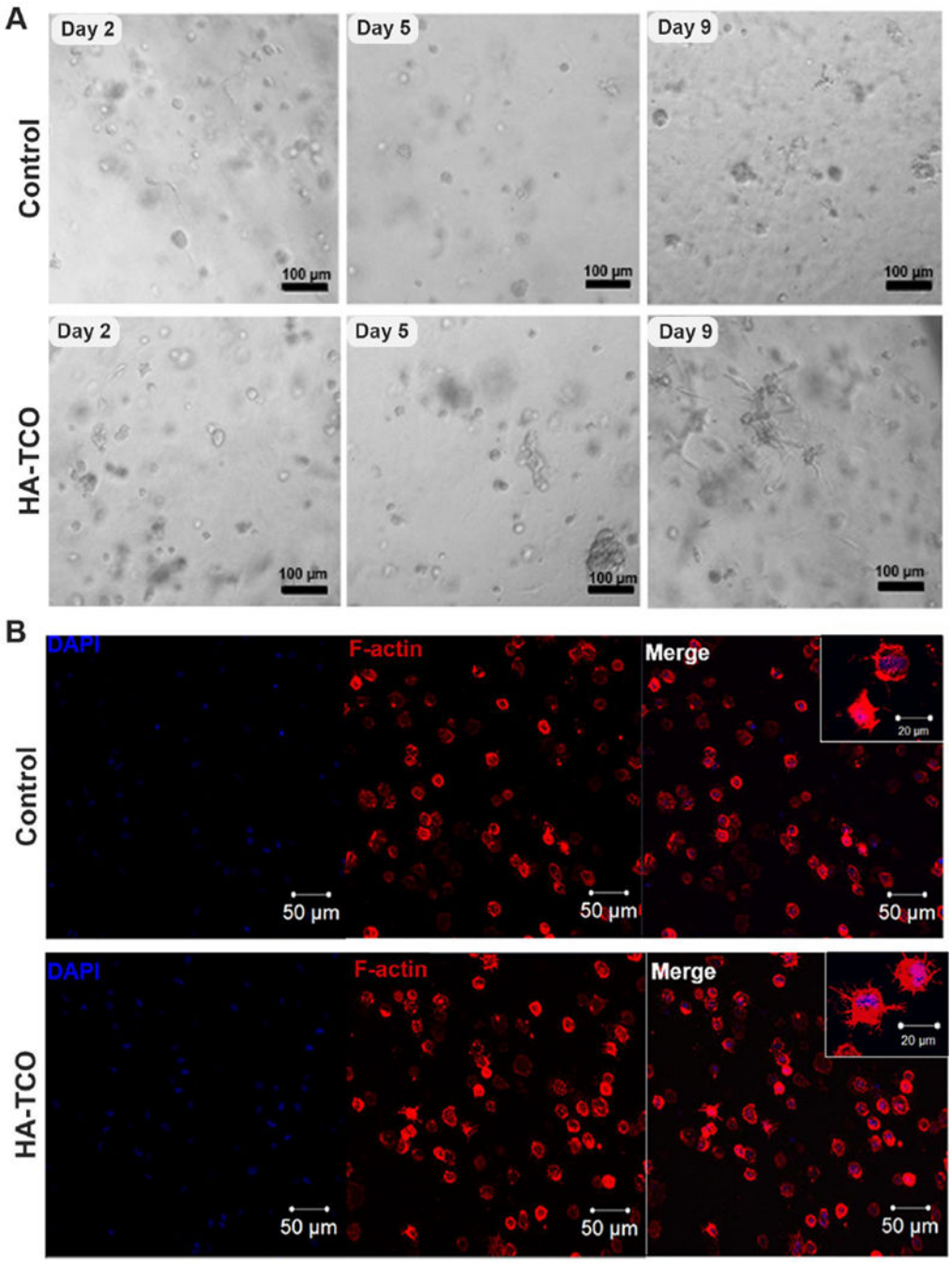

Figure 5.

Effect of tetrazine ligation-mediated matrix stiffening on hMSC morphology. Cells were initially encapsulated in MMP-degradable Michael gels. Two days later, HA-TCO were introduced to the growth media. Cultures were maintained until day 9. (A): Time series brightfield images of hMSC cultured in HA/POM gels with and without HA-TCO treatment. (B): Representative confocal images of fluorescently stained hMSCs after 9 days of culture with or without the HA-TCO treatment. Cell nuclei and F-actin were stained blue and red, respectively.

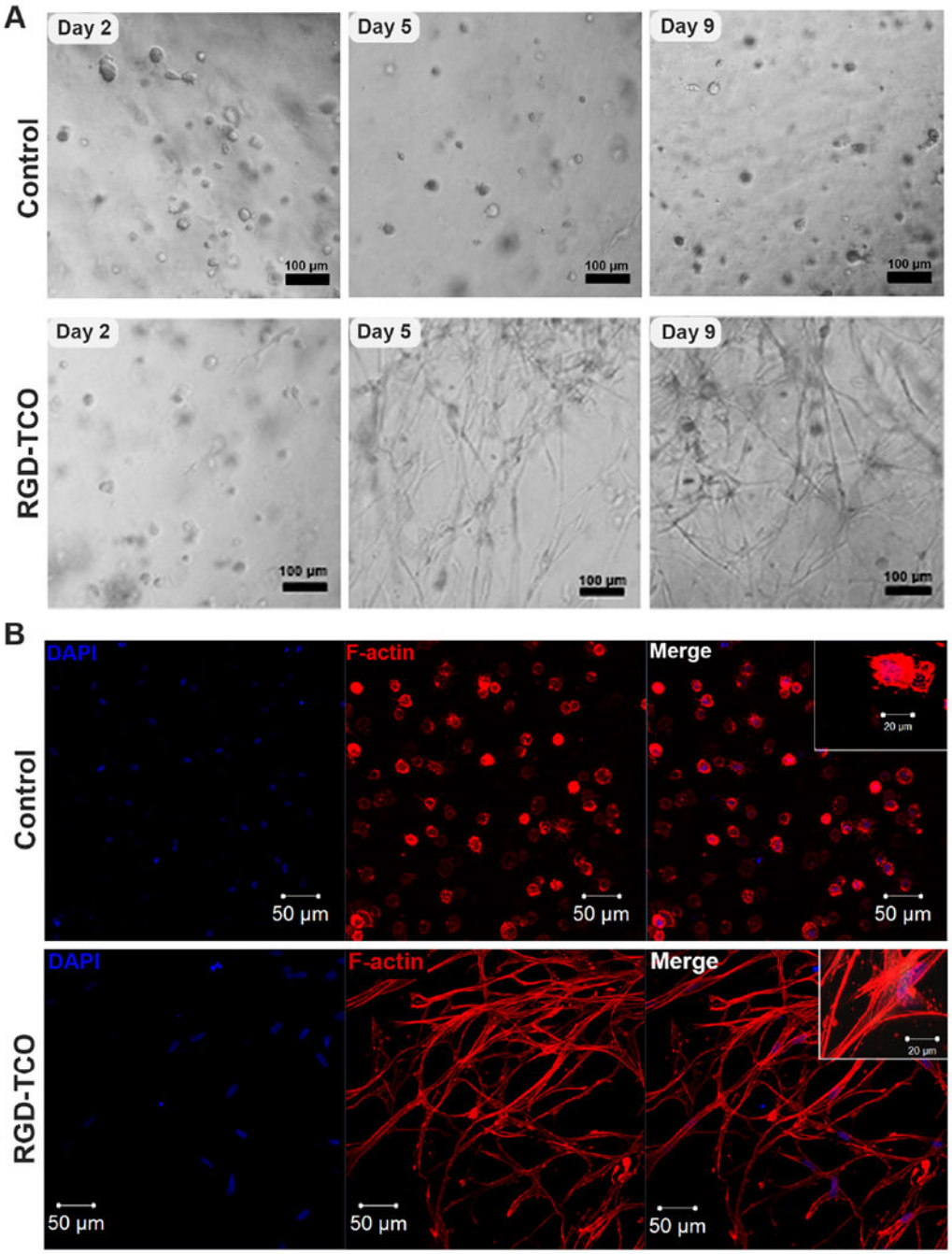

Figure 6.

Effect of tetrazine ligation-mediated RGD tagging on hMSC morphology. Cells were initially encapsulated in MMP-degradable Michael gels. Two days later, RGD-TCO (2 mM) were introduced to the growth media. Cultures were maintained until day 9. (A): Time series brightfield images of hMSC cultured in HA/POM gels with or without RGD-TCO treatment. (B): Representative confocal images of fluorescently stained hMSC after 9 days of culture with or without RGD-TCO treatment. Cell nuclei and F-actin were stained blue and red, respectively.

Gene	Forward Primer (5'-3')	Reverse Primer (5'-3')	GeneBank#	Efficiency	Product Size (bp)
GAPDH	GAAATCCCATCACCATCTTCCAGG	GAGCCCCAGCCTTCTCCATG	NM_001289746	2.08	120
COL3A1	TGGTGCCCCTGGTCCTTGCT	TACGGGGCAAAACCGCCAGC	NM_000090	2.03	87
COL1A1	AATGGTGCTCCTGGTATTGCTGGT	ACCAGTGTCTCCTTTGCTGCCA	XM_005257058	2.10	141
TNC	GGGCTGGTTGTATTGATGCTTT	AGGGACCACTGGGTGAGAGA	XM_005251975	2.0	76
FN	ACCTACGGATGACTCGTGCTTTGA	CAAAGCCTAAGCACTGGCACAACA	NM_001306132	2.10	116
MMP1	GGGAGATCATCGGGACAACTC	GGGCCTGGTTGAAAAGCAT	NM_001145938	2.03	72
FSP-1	AGCTTCTTGGGGAAAAGGAC	CCCCAACCACAT CAGAGG	NM_019554	1.98	200
aP2	AACCTTAGATGGGGGTGTCCTG	TCGTGGAAGTGACGCCTTTC	NM_001442	2.1	125
ACAN	TCGAGGACAGCGAGGCC	TCGAGGGTGTAGCGTGTAGAGA	NM_013227	2.03	85
ALP	GCCTACCAGCTCATGCATAAC	GAAGTGGGAGTGCTTGTATCT	NM_000478	2.07	192
αSMA	CCAAGCACTGTCAGGAAT	AGGCAGTGCTGTCCTCTT	NM_001613	1.99	60

A

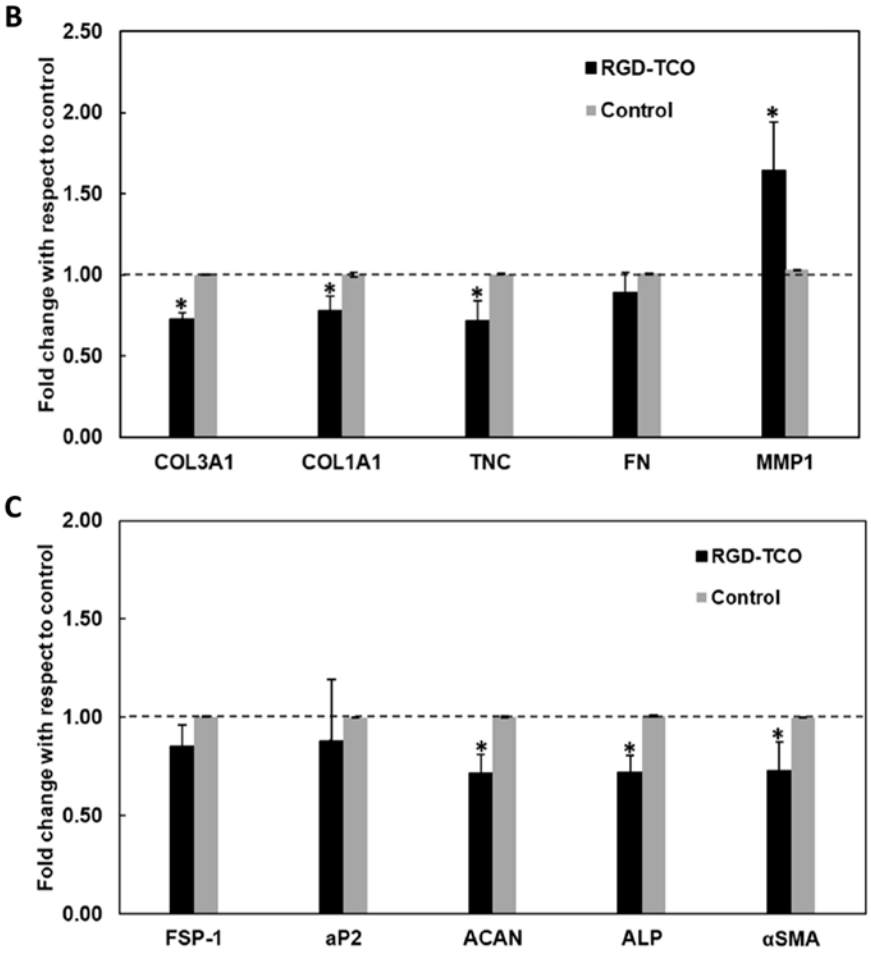

Figure 7.

Effect of tetrazine ligation-mediated RGD tagging on hMSC phenotype as assessed by qPCR. Cells were initially encapsulated in MMP-degradable Michael gels. Two days later, RGD-TCO (2 mM) were introduced to the growth media. (A): Summary of primer information; (B): qPCR analyses of genes encoding essential ECM proteins: COL3A1, COL1A1, TNC, FN and MMP1. (C): qPCR analyses of genes encoding classic hMSCs differentiation markers: FSP1, aP2, ACAN, ALP and αSMA. The relative gene expression (fold change) was normalized to the RGD-free controls (baseline). *significant difference (p

< 0.05) between control and RGD-TCO. Error bars represent SEM. Gene abbreviations: GAPDH, glyceraldehyde-3-phosphate dehydrogenase; COL3A1, collagen III alpha 1 chain; COL1A1, procollagen I alpha 1 chain; TNC, tenascin-C; FN, fibronectin; MMP1, matrix metalloproteinase 1; FSP1, fibroblast specific protein-1; aP2,adipocyte Protein 2; ACAN, aggrecan; ALP, alkaline phosphatase; αSMA, alpha smooth muscle actin.